Numerical Simulations of a Tornadic Supercell over the Mediterranean

MARIO MARCELLO MIGLIETTA

ISAC-CNR, Lecce, Italy

JORDI MAZON

Department of Physics, Universitat Politecnica de Catalunya–BarcelonaTech, Barcelona, Spain

RICHARD ROTUNNO

National Center for Atmospheric Research,[a] *Boulder, Colorado*

(Manuscript received 27 December 2016, in final form 7 March 2017)

ABSTRACT

On 28 November 2012, a multivortex EF3 tornado occurred in southeastern Italy causing one fatality and estimated damage of 60 million euros. At approximately 1050 LT (0950 UTC), this tornado, which initially formed in association with a supercell thunderstorm over the Ionian Sea, moved inland. The environment where the tornadic supercell developed was characterized by large vertical wind shear in the lowest 1 km of the atmosphere and moderate conditional instability. Mesoscale-model numerical simulations show that it is possible to produce a simulated supercell thunderstorm with a track, change in intensity, and evolution similar to the actual one that spawned the tornado in Taranto, southern Italy. The genesis of the simulated supercell is due to a combination of mesoscale meteorological features: warm low-level air advected toward the Ionian Sea, combined with midlevel cooling due to an approaching trough, increased the potential instability; the intense vertical shear favored the possibility of supercell development; and boundary layer rolls over the Ionian Sea moved in phase with the cells produced by the orography of Calabria to supply ascent, moisture, and heat to the convection. An unusual feature of the present case is the central role of the orography, which was verified in a sensitivity experiment where it was reduced by 80%.

1. Introduction

Although not generally known, there is a rich history of tornado activity in Italy (Peterson 1998). Recently, the occurrence of several intense tornadoes in Italy has produced renewed interest in the phenomena. For example, on 8 July 2015, an EF4 tornado struck an area near Venice, causing one death and 72 injuries and completely destroying a villa that dated back to the seventeenth century (ARPAV 2015). A multivortex EF3 tornado hit Taranto, in southeastern Italy, on 28 November 2012, and was responsible for one death and estimated damage of 60 million euros (Miglietta and Rotunno 2016, hereafter MR16). A numerical simulation of the meteorological causes for the severe weather in this case using the Weather Research and Forecasting (WRF) Model is the subject of the present study.

Most studies of tornadogenesis in the Mediterranean have focused on mesoscale and synoptic-scale observations. Bech et al. (2007) found that a mesoscale convergence line in a highly sheared and relatively low-instability environment was responsible for a tornado outbreak near Barcelona, Spain, during September 2005. Bertato et al. (2003) found the thermal boundary generated by previous storm outflows and their modification by orography could have played an important role in producing a tornado in the foothills of northeastern Italy. Similarly, Aran et al. (2009) identified a low-level thermal boundary, related to warm-air advection, evaporational cooling due to precipitation, and differential cooling due to cloud cover, in the environment where an F2 tornado developed in the Catalonia region of Spain. Mateo et al. (2009) found that the convergence lines induced by the local orography were

[a] The National Center for Atmospheric Research is sponsored by the National Science Foundation.

Corresponding author: Mario Marcello Miglietta, m.miglietta@isac.cnr.it

DOI: 10.1175/WAF-D-16-0223.1

probably the main factor in a tornado outbreak in northeastern Spain. Nastos and Matsangouras (2014) identified specific synoptic weather patterns favorable for tornado occurrence in western Greece. A comprehensive documentation of tornadoes over Europe can be found in Antonescu et al. (2016).

Synoptic and observational analyses are valuable for identifying environments favorable for supercells. Additionally, high-resolution simulations by means of limited-area meteorological models (LAMs) may help us to understand the mechanisms behind the triggering and development of the supercells and to explore their sensitivity to different parameters. The growth in computational resources combined with more accurate LAMs has allowed the reduction of the typical horizontal grid spacing down to $O(1)$ km even for operational runs. However, as the predictability limit for individual convective-scale elements is at most a few hours (Lilly 1990), in the absence of strong forcing the precise location and timing of convection may be difficult to simulate at a lead time of more than an hour or so, even at such high spatial resolution. Fortunately, in many cases severe convection occurs in association with larger mesoscale flow features, which may have greater predictability. The use of ensemble forecasts has shown promise in estimating the probability of such convective events (Schwartz et al. 2015). In these cases, although operational-like simulations cannot simulate tornadoes, they can often identify the mesoscale forcing conducive to the genesis of supercells, which are known to produce the most severe tornadoes.

The need for high-resolution simulations is particularly evident in inhomogeneous environments like that of the Mediterranean basin. Indeed, considering that many tornadoes occur near the Mediterranean coast, which is surrounded by steep mountains, we expect that the interaction with the orography, the land–sea contrast, and the intense air–sea interaction are important in the Mediterranean environment (Lionello et al. 2006), determining significant meso-β- and meso-γ scale variations of the relevant instability parameters. This is very different from the more homogeneous, synoptic-scale setting typical for the severe convective weather of the U.S. Great Plains (Doswell et al. 2012). For example, high-resolution numerical simulations of a tornadic event in eastern Spain (Homar et al. 2003) showed that small-scale terrain features, as well as solar heating, were crucial in forcing intense small-scale circulations favoring the development of severe convection. Recently, Miglietta et al. (2016) noted that the evolution of a supercell in northeastern Italy was controlled by the synchronous movement of a tongue of air with high equivalent potential temperature θ_e from the Adriatic Sea with the propagation speed of a supercell. The foregoing are distinctive features of Mediterranean supercells as compared with supercells of the Great Plains, where the pattern of θ_e is generally more homogeneous.

To our knowledge, there are very few studies dealing with the effect of mountains on supercell triggering and development. In idealized conditions, Markowski and Dotzek (2011) showed that the orography mainly changes the thermodynamic conditions (affecting convective inhibition and relative humidity) as a consequence of the flow over/around the mountain. Bosart et al. (2006) studied an F3 tornado in Massachusetts and found that the topography, and in particular the channeling of low-level flows, conspired to create local enhancements to tornadogenesis potential and to compensate for the increased friction over the orography. Recently, Matsangouras et al. (2012, 2014, 2016) showed that, for some tornadoes over Greece, the presence of steep mountains may represent an important factor for tornadogenesis, by changing the values of some instability parameters compared with a simulation with no orography. Here, the synoptic-scale/mesoscale features responsible for the triggering of the supercell in Taranto are analyzed. We believe this topic is worthy of investigation, considering we are not aware of any paper showing that the perturbations induced by a mountain may favor the downstream triggering and the location of a supercell, as found and described in the present study.

This paper is organized as follows. Section 2 contains a short summary of the available observations. Section 3 describes the present nested-grid numerical simulations pertaining to the meteorological conditions surrounding the Taranto tornado of 28 November 2012, while section 4 provides a synoptic overview for this case. Section 5 describes the results of the numerical experiment in the inner grid, focusing on the mesoscale mechanisms responsible for the genesis and development of the supercells. As the orography of Calabria (at the southernmost tip of Italy) appears to play a key role in triggering convection, an additional experiment with reduced orography is also analyzed. Conclusions are drawn in section 6.

2. Observations

A comprehensive description of the tornado affecting Taranto is discussed in MR16, so only a short overview is provided here. (Figure 1 identifies the places mentioned herein.) Several videos and pictures document this severe weather event and can be easily found online. Movies clearly show that the tornado originated over the Ionian Sea, near the port of Taranto, which was still warm at the end of November (the sea surface

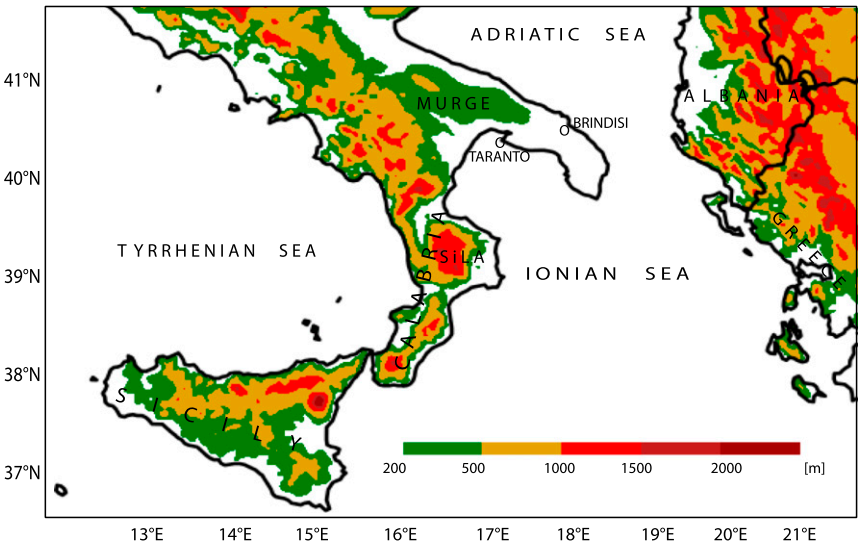

FIG. 1. Names and locations of the places mentioned in the text. The orography in domain 2 is also shown.

temperature measured in the area was 18.7°C). Tornado landfall occurred at 0950 UTC (1050 local time) near the largest steel plant in Europe, a couple of kilometers from Taranto. A crane weighing several tons was knocked down; unfortunately, an employee working on the crane was killed. In this phase, the tornado reached its greatest intensity, at least EF3 according to an estimation of the degree of damage (McDonald and Mehta 2006), with a total estimated damage of 60 million euros.

After landfall, the movement of the tornado's parent supercell was observed to slightly change from SSW–NNE to S–N (Fig. 5 in MR16). The track of the associated tornado observed over land can be identified in Fig. 2a (blue and pink dots). The translational velocity of the supercell is estimated to be $\sim 22\,\mathrm{m\,s^{-1}}$ from the nearby 1200 UTC sounding in Brindisi (Fig. 3a). The funnel width was evaluated as approximately 300 m, with several satellite vortices (Venerito et al. 2013). Moving inland, the tornado weakened only slightly, destroying the canopy of a gas station in the town of Statte, about 12 km north of Taranto, and increased its diameter up to 500 m. Just afterward, the vortex no longer extended fully to the surface as no damage was reported during the passage of the supercell across the Murge hills (peak altitude of approximately 700 m). However, on the northeastern (lee) side of the Murge hills the supercell intensified again and produced some significant tornadic damage (although weaker than before) near the Adriatic coast. The overall horizontal extent of the overland track of the supercell was about 50 km and the duration about 50 min.

The radar reflectivity mosaic from the Italian Civil Protection Agency shows a series of convective cells elongated in the direction of the 500-hPa wind from the orography of Calabria (Fig. 3b), which appears to have played an important role in the event. Another remarkable feature, emerging from the Brindisi sounding at 1200 UTC (Fig. 3a), is the intense low-level wind shear [the wind speed changes from 12 kt ($1\,\mathrm{kt} = 0.51\,\mathrm{m\,s^{-1}}$) at 10 m to 56 kt at about 700 m], so that in the lowest 1 km the storm-relative helicity (SRH) was $553\,\mathrm{m^2\,s^{-2}}$ and the energy–helicity index (EHI) reached the high value of 2.7. On the other hand, only moderate instability was present in the sounding, as the convective available potential energy (CAPE) was slightly less than $1000\,\mathrm{J\,kg^{-1}}$. The extremely high values of the surface–1-km wind shear in the proximity sounding (about $25\,\mathrm{m\,s^{-1}}$), combined with the low lifting condensation level (about 700 m), is unusual compared with the soundings of Great Plains tornadoes [cf. with Fig. 3a in Brooks et al. (2003), and with Fig. 10.13 in Markowski and Richardson (2010)], while it is more similar to that of strong/violent tornadoes in the southeast United States (Grams et al. 2012). Also, as compared with the only climatology of tornadoes available for Italy (Giaiotti et al. 2007), the sounding in the present case shows some unusual features, such as the largest values of EHI and SRH in the entire dataset, and low-level wind shear twice as large as the mean climatological value for F3 tornadoes.

3. Numerical simulations

Version 3.5.1 of the WRF-ARW (see www.wrf-model.org; Skamarock et al. 2008) is used to simulate the event. WRF is a numerical weather prediction system, which

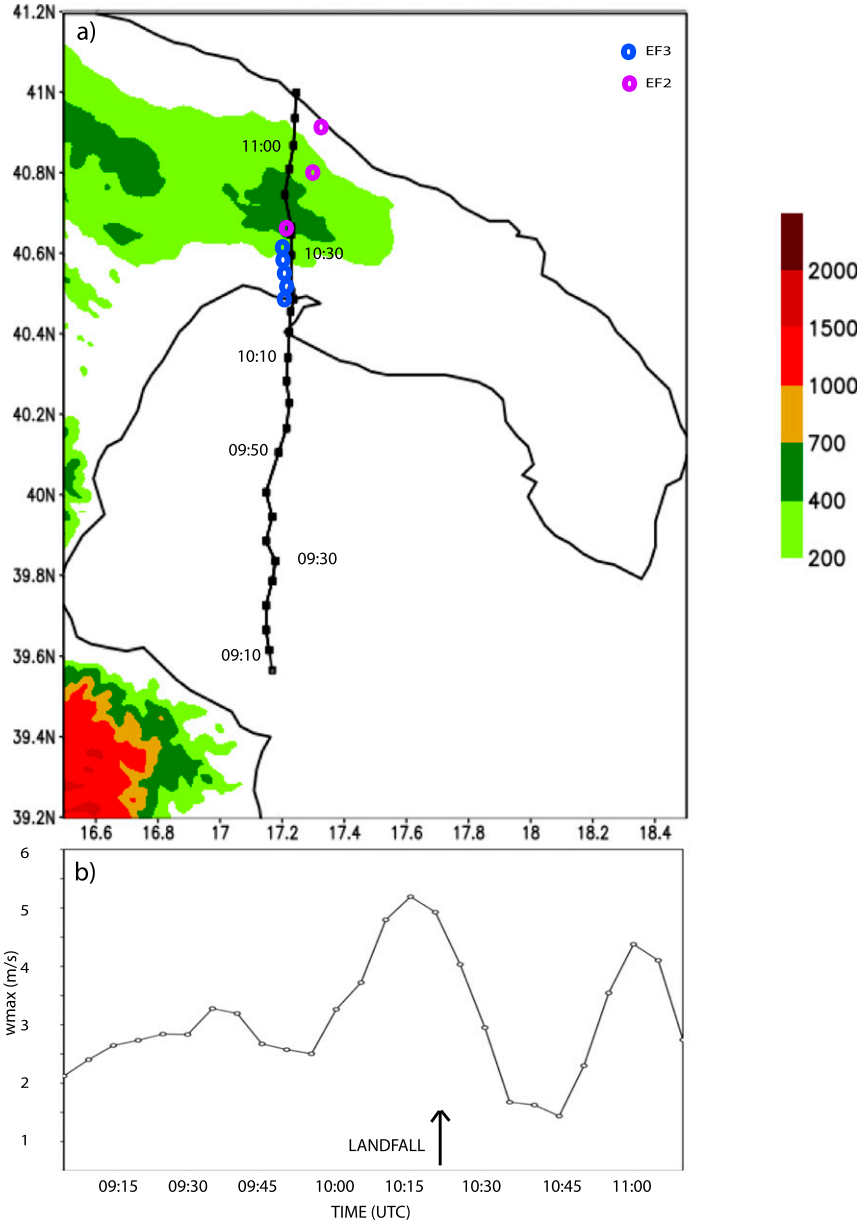

FIG. 2. WRF Model simulation in domain 3: (a) track of the observed and the simulated supercell that would have produced the Taranto tornado (orography in colors; m) and (b) maximum vertical velocity at 950 hPa evaluated in the window 39.6°–41.2°N, 17.0°–17.5°E. A track could not be clearly identified during the crossing of the Murge hills.

solves the fully compressible, nonhydrostatic primitive equations. Terrain-following-type sigma coordinates are used in the vertical, where here 40 levels are employed, with levels more closely spaced near the ground to better resolve the boundary layer (their vertical distance ranges from 58 m in the boundary layer to 600 m in the lower stratosphere). Model output is saved every 5 min to follow in detail the time evolution of the supercell, whose lifetime is approximately 1 h.

Three one-way-nested domains are implemented, as shown in Fig. 4. The outer domain covers the southern part of the central Mediterranean (210 × 150 grid points, $dx = 9$ km), while the intermediate domain covers southern Italy, Albania, and western Greece (271 × 193 points, $dx = 3$ km); the inner domain covers the Ionian regions of southern Italy (211 × 271 points, $dx = 1$ km). The region affected by the supercell is in the middle of the inner domain, and on the eastern side of the two

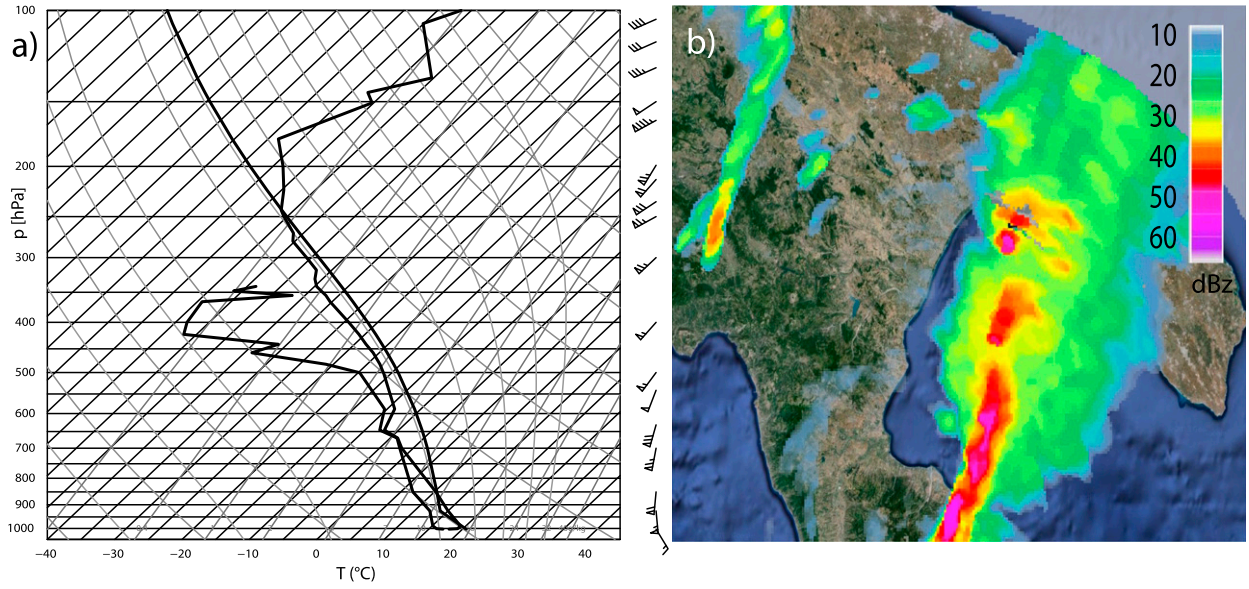

FIG. 3. (a) Skew T diagram in Brindisi at 1200 UTC 28 Nov 2012 (wind in kt; source: University of Wyoming). (b) Radar reflectivity (vertical maximum intensity) at 0945 UTC (source: Italian Civil Protection Department, Presidency of the Council of Ministers) enlarged over the Ionian regions.

coarser domains, considering that the propagation of the synoptic-scale features is from the west.

Considering the successful simulations of a supercell near the Mediterranean coast (northeastern Italy) discussed in Miglietta et al. (2016), we employ the same parameterization schemes, which include the Thompson et al. (2008) scheme for microphysics; the Rapid Radiative Transfer Model for longwave radiation (Mlawer et al. 1997) and the Dudhia (1989) scheme for shortwave radiation; the unified Noah model (Niu et al. 2011) for land surface interactions; and Mellor–Yamada–Janjić, a turbulent kinetic energy closure scheme, for the planetary

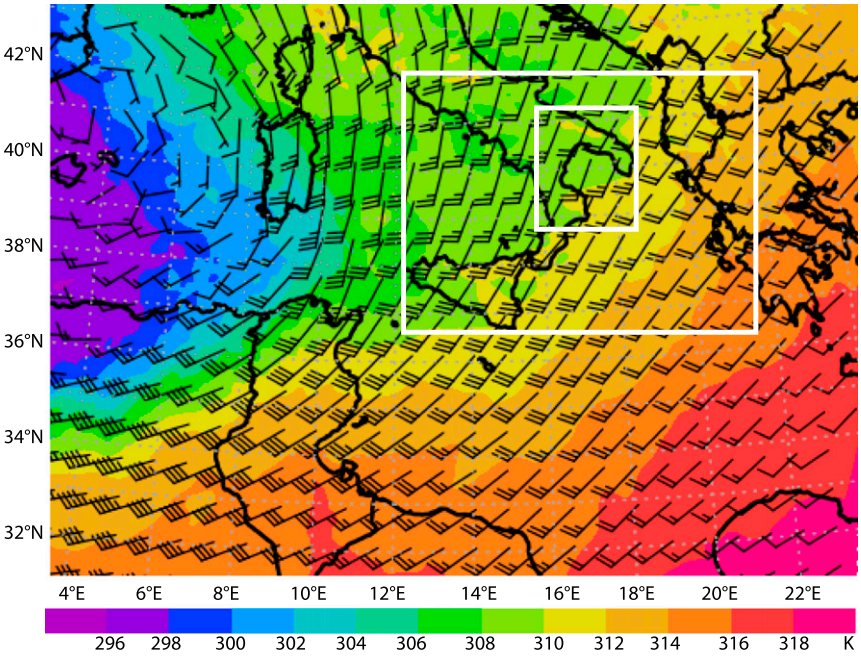

FIG. 4. WRF Model simulation, domain 1. Shown are wind vectors (m s^{-1}; barbs, long bar is 10 m s^{-1} and short bar is 5 m s^{-1}) and θ (K; color scale) at 500 hPa at 0900 UTC 28 Nov 2012. Model domains are also shown.

boundary layer (Janjić 2001); finally, cumulus convection is treated explicitly in all domains.

Different initial/boundary conditions (the boundary conditions are updated every 3 h) were initially tested, changing both the large-scale forcing—the Integrated Forecasting System (IFS) of the European Centre for Medium-Range Weather Forecasts (ECMWF) versus the Global Forecasting System (GFS) analysis/forecasts—and the initial time for the simulations (0000 and 1200 UTC 27 November 2012 and 0000 UTC 28 November 2012). The only simulation to reproduce the supercell was the one starting at 0000 UTC 27 November 2012, which was forced with the ECMWF IFS analysis/forecasts and only this run will be analyzed in the following. [As discussed in Miglietta et al. (2016), the proper simulation of a supercell in the Mediterranean requires that the small-scale variations in space and time of the mesoscale features responsible for it are properly simulated, so that an ensemble approach appears unavoidable for correctly simulating this kind of event.]

Other simulations are performed to better understand the role of the orography of Calabria in triggering the supercell. The sensitivity experiments are implemented as the control run but with the mountain height reduced in all domains. In this way, the changes in the inner domain can be ascribed mainly to the contribution of the orography of Calabria, since the evolution of the large-scale weather patterns in the control run is retained.

4. Synoptic conditions

Synoptic features are analyzed using the WRF Model fields in the outermost domain. Figure 4 shows the wind and the potential temperature at 500 hPa at 0900 UTC 28 November 2012, just before the supercell formed. A cold upper low over the western Mediterranean, approaching Italy from the west, is associated with a southwesterly flow in the Ionian regions of Italy, located on the eastern side of a slightly diffluent trough. As a consequence of the eastward propagation of these synoptic patterns, the local 500-hPa wind speed progressively intensifies up to 30 m s^{-1} during the simulation, while warm air of African origin, affecting all of southern Italy at the beginning of the simulation, is confined to the eastern Mediterranean basin. At 0900 UTC, the Ionian regions are still far from the large-scale trough (and its coldest core) over the Tyrrhenian Sea, though the incoming cold air produces a significant cooling in the midtroposphere a few hours before the event.

The synoptic features are seen at low levels, in particular the wind vectors and the equivalent potential temperature θ_e at 1000 hPa, together with the wind vectors at 900 hPa (to show that the boundary layer wind is veering with height) at 0000 UTC (Fig. 5a) and at 0900 UTC (Fig. 5b). Comparing the two panels, one can see the intensification of a south-southeasterly low-level jet (up to 25 m s^{-1}), bringing warm and moist air toward southern Italy, and in particular over the Ionian Sea, ahead of the cold front, which at 0900 UTC appears to be located near Sardinia. Thus, the combination of warm, humid low-level air and cooler, midlevel air makes atmospheric conditions favorable for potential instability, as shown below in Fig. 6 (i.e., it increases the CAPE in the area).

The alternating warmer and cooler strips simulated along the east side of the warm tongue appear elongated in the direction of the low-level shear (approximately east-northeastward). This pattern is likely related to convectively induced circulations (i.e., rolls, possibly associated with individual convective cells elongated in the shear-parallel direction). Ching et al. (2014) showed that the horizontal variations in these modeled fields are grid-size dependent, since the grid spacing of $O(1)$ km is within Wyngaard's (2004) turbulence "terra incognita."

To explain why the horizontal convective rolls develop only on the northeastern side of the warm tongue, Fig. 6 shows the vertical sounding in the lower troposphere, from 1000 to 500 hPa, at 0900 UTC, simulated at two locations (indicated by the circles in Fig. 5b), respectively, southeast of Calabria (38.0°N, 18.5°E) and farther south (35.0°N, 18.5°E), near the African coast. Only at the former point are rolls generated in the simulation. The wind profiles appear similar; in particular, the intense deep-layer shear appears favorable to supercells in both cases. However, there are significant differences in the boundary layer temperature and dewpoint temperature profiles. At the northern point (Fig. 6, black solid lines), the air is more humid in the low levels and close to saturation, so that low-level parcels (Fig. 6, cyan solid line) encounter only a small convective inhibition, even in the presence of a shallow inversion at 850 hPa. At the southern point (Fig. 6, black dashed lines), the low-level air is much drier and there is a prominent inversion, which increases the convective inhibition (and similarly for the west side of the warm tongue). The difference in the humidity content can be explained considering the longer transit over the sea of the low-level air reaching the northern point, which favors a longer duration of moistening of boundary layer air parcels, as discussed in Moscatello et al. (2008). The profiles of temperature at an earlier time (0300 UTC) show that both points were unstable in the boundary layer (not shown); however, the boundary layer in the northern location

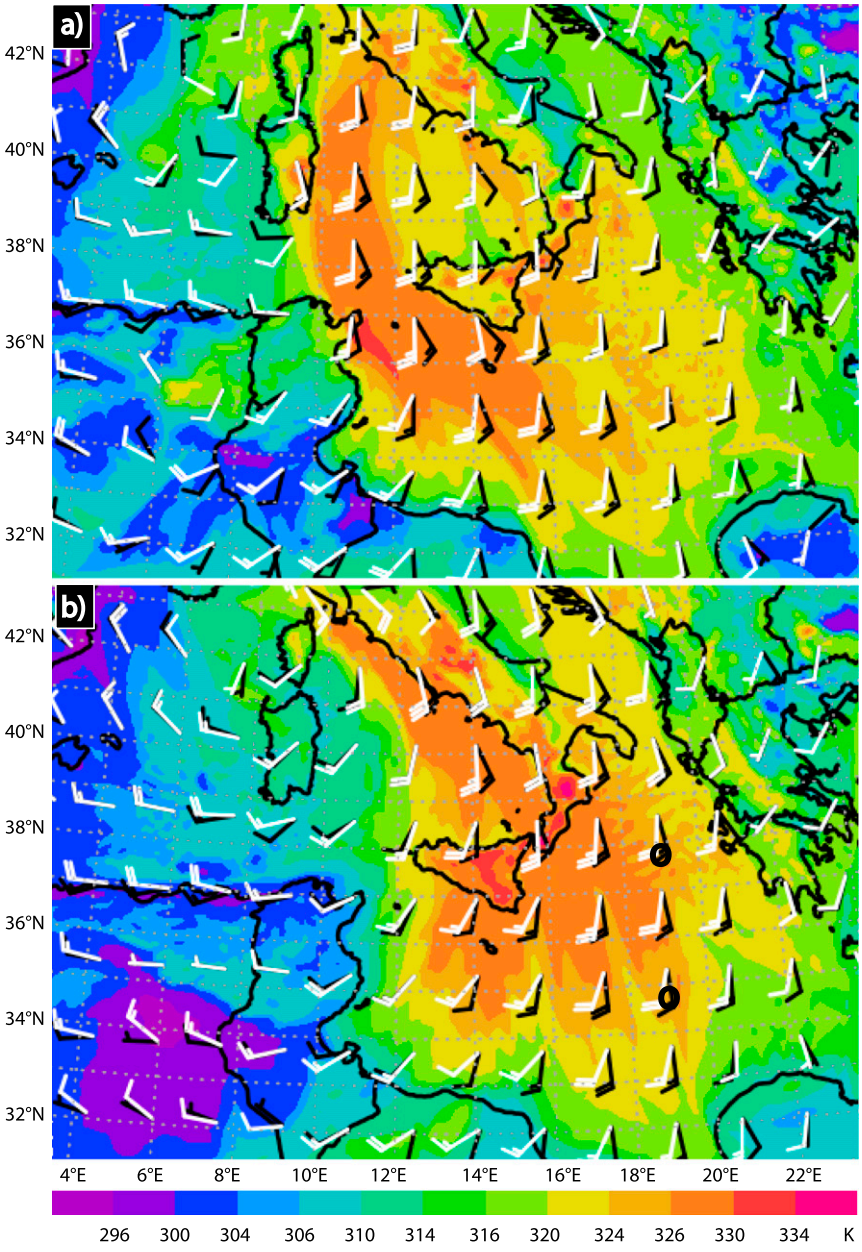

FIG. 5. WRF Model simulation, domain 1. Wind vectors (m s^{-1}; black barbs) and θ_e (K; color scale) at 1000 hPa at (a) 0000 and (b) 0900 UTC 28 Nov 2012. The wind vectors at 900 hPa (m s^{-1}; white barbs) are also shown to indicate that the boundary layer wind is veering with height. The locations of the soundings shown in Fig. 6 are indicated by the O marks. Values of θ_e are locally extrapolated below the ground.

was colder, being located farther east of the trough and less affected by low-level warm-air advection. In the following hours, both locations were affected by intense warm-air advection (cf. Fig. 5a with Fig. 5b); however, only at the southern point was the temperature increase above the boundary layer sufficient to generate an inversion strong enough to inhibit convection, while at the northern point the air remained relatively cooler, so that convective inhibition remains very small.

5. Mesoscale analysis

The analysis in the previous section identified a large-scale environment favorable to convection and supercell development. A closer examination of the inner model

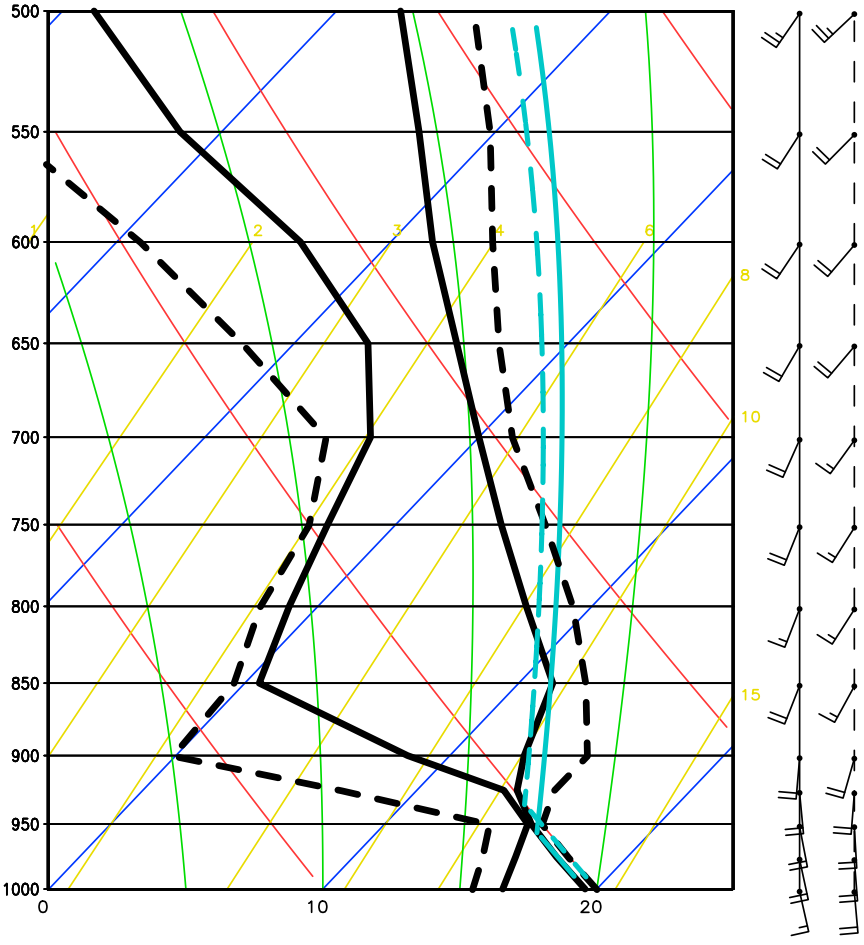

FIG. 6. Vertical profiles of temperature, dewpoint, and wind ($m\,s^{-1}$; barbs) (WRF Model simulation, domain 3) from 1000 to 500 hPa at 0900 UTC, simulated at two locations (shown in Fig. 5b by O marks), respectively, southeast of Calabria (38.0°N, 18.5°E; solid line, left wind profile) and farther south (35°N, 18.5°E; dashed line, right wind profile), near the African coast. Only at the former point are convective rolls generated in the simulation.

domain is necessary to identify the presence of local forcing, which may have played an important role as well.

a. Mesoscale environment

Figure 7 shows the 1000- and 900-hPa wind vectors and θ_e at 0700 UTC (Fig. 7a) and at 1000 UTC (Fig. 7b), that is, just before the tornado landfall; the advection of warm, moist air along the Ionian Sea is apparent and makes the environment more unstable, while east–west-oriented bands of warmer (in terms of θ_e) air move northward from the southeastern side of the domain and represent the signature of the previously identified rolls. The intensification of the 900-hPa wind (reaching around $25\,m\,s^{-1}$) increases the low-level shear, making the environment very favorable for supercell tornadogenesis.

The intense northward transport of high-θ_e air is modulated by the presence of Calabria, which diverts the low-level jet and the warm-air advection from the northwestern Ionian coast (Fig. 7a). Indeed, the blocking of the southerly flow by the orography produces a weak cyclonic circulation in the lee, at around 39.9°N, 16.25°E, separated from the main flow (Smolarkiewicz and Rotunno 1989). The vortex shedding is consistent with the value of the Froude number Fr, the parameter that roughly estimates the way the flow interacts with the orography (Smith 1979). Considering $U \approx 15\,m\,s^{-1}$ as the environmental wind impinging on the mountain, $N \approx 10^{-2}\,s^{-1}$ the Brunt–Väisälä frequency of the incoming airflow, and $h \approx 2000\,m$ as an estimate of the mountain height, we obtain $Fr = U/(N \times h) \approx 0.7$. Since $Fr < 1$, the environmental conditions appear favorable for flow blocking. At 1000 UTC, the region to the north of Calabria's orography still appears sheltered from the main flow: the low-level air, although warmer, is still

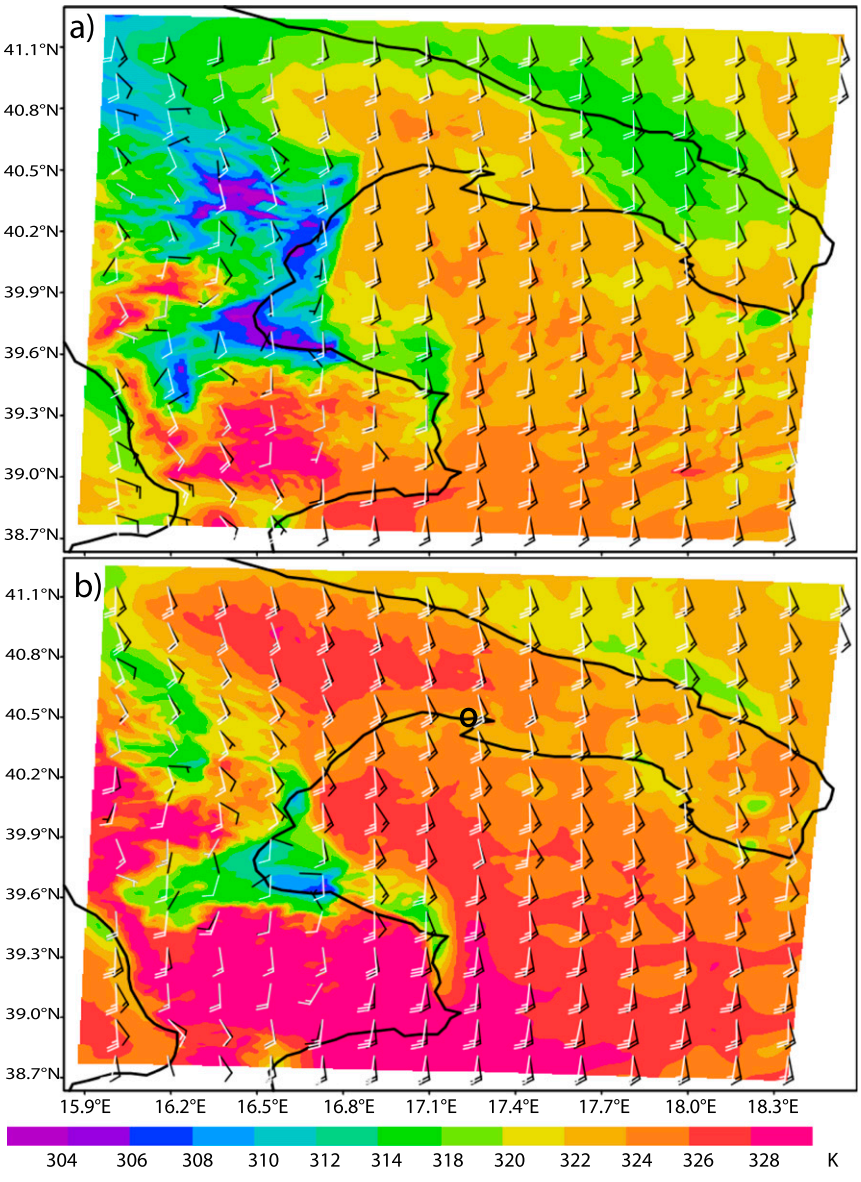

FIG. 7. WRF Model simulation, domain 3. Shown are wind vectors at 1000 hPa (m s^{-1}; black barbs) and 900 hPa (m s^{-1}; white barbs) and θ_e at 1000 hPa (K; color scale) at (a) 0700 and (b) 1000 UTC 28 Nov 2012. The location of the tornado landfall is indicated by O in (b). Values of θ_e are locally extrapolated below the ground.

cooler than the air advected by the southerly flow over the sea. Some cooler (light orange) spots in the θ_e field, near the Ionian coast of Apulia, are associated with the outflow of convective cells developing over the sea.

The presence of these cells can be better identified in Fig. 8, which shows a perspective view of the maximum reflectivity (in dBZ) and the 100-m wind at 0830 UTC (Fig 8a) and 1000 UTC (Fig 8b). At the earlier time (Fig. 8a), the cells appear aligned in the direction of the low-level shear (west-southwest–east-northeast) as they move northward, extending in a linear pattern from Calabria to the southern tip of Apulia across the Ionian Sea. Inland, some cells are generated by the uplift induced by the orography of Calabria, but at this time they remain confined over the mountains. Later, a series of cells extends north of the Sila mountains, triggered by the orography and advected northward by the lower-to-midtropospheric wind. At 1000 UTC (Fig. 8b), some cells appear elongated from the Sila mountains toward Taranto, in a way similar to the radar reflectivity observations (Fig. 3b), although the simulation underestimates the areal coverage of the

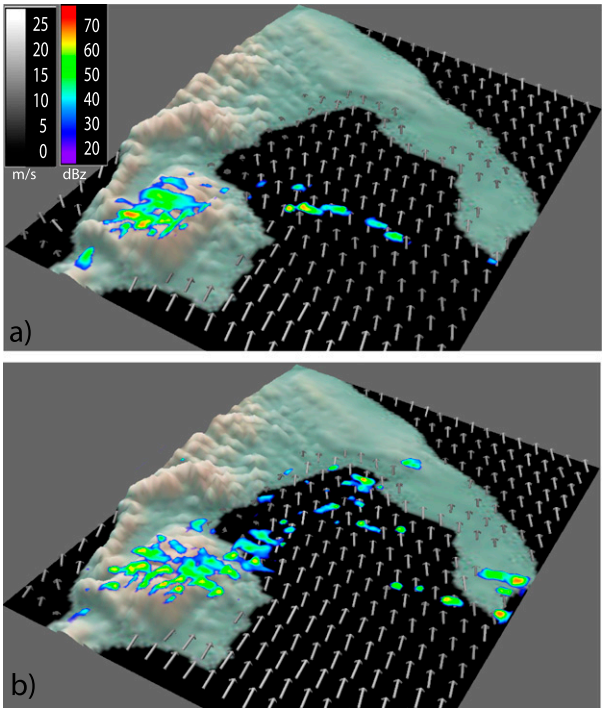

FIG. 8. WRF Model simulation, domain 3. Shown are wind vectors at 100-m height (m s^{-1}; grayscale) and maximum reflectivity (dBZ; color scale) at (a) 0830 and (b) 1000 UTC 28 Nov 2012.

convection. This kind of solution (downwind cells) should be expected from the theory of conditionally unstable flows over orography (Miglietta and Rotunno 2009): the ratio of the advective time scale $\tau_a = a/U$ to the convective time scale $\tau_c = h_t/(\mathrm{CAPE})^{1/2}$ (the time that convective elements take to grow and produce rain at the ground), where U is the wind speed, a the ridge half-width, and h_t the tropopause height), can be calculated considering a profile at a point located upstream of Sila (e.g., at the point 38.5°N, 17.0°E at 0900 UTC). We obtain $\tau_a/\tau_c \sim 6$, which means that the environmental conditions favor a regime characterized by quasi-stationary convective cells on the upstream side and a second set of convective cells generated downwind (middle panel of Fig. 8 in Miglietta and Rotunno 2009).

The most intense of these cells, the one that is to become the simulated Taranto supercell (identified in Fig. 8b by the area of high dBZ approaching Taranto), forms over the sea just in the lee of the orography of Calabria at around 0905 UTC, and progressively intensifies as it moves toward the coastline of Apulia (Fig. 2b). The location of the simulated supercell reaches Taranto only 30 min later than the observed supercell (1020 vs 0950 UTC) and just 1–2 km from its track estimated in Fig. 1 of MR16. The simulated supercell translation speed is approximately 24 m s^{-1}, which is also consistent with the observations.

The trajectory of the cell can only be easily identified beginning from approximately 30 min before landfall (at 0935 UTC). Earlier, one can identify the original cell at 0905 UTC, which then splits four times into a pair of left and right movers (Weisman and Klemp 1982); taking into account this complication, the full track of the storm can be roughly identified by the

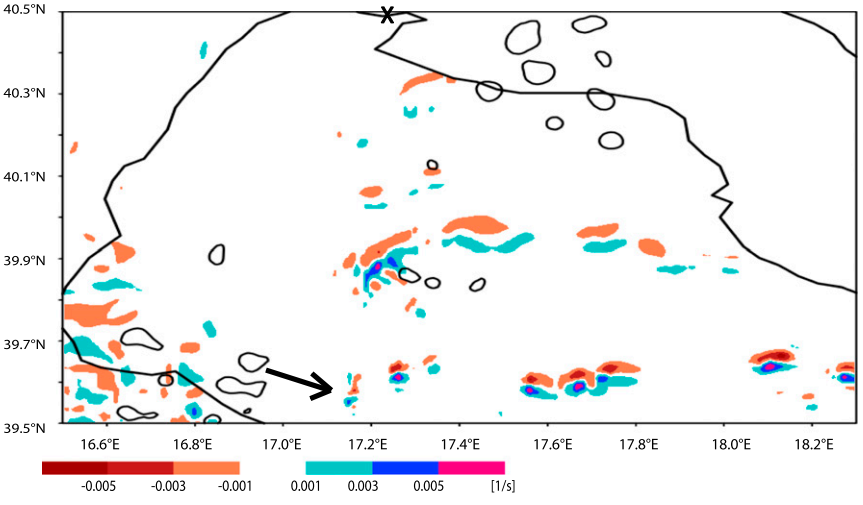

FIG. 9. WRF Model simulation, domain 3. Shown is the 800-hPa vertical vorticity (shaded; s^{-1}) at 0905 UTC 28 Nov 2012. The contour of cloud water content = 0.5 g kg^{-1} at 500 hPa (solid thick line) is also shown. The location of the vorticity perturbation that is going to develop into the supercell is shown with an arrow; the location of the landfall is indicated by X.

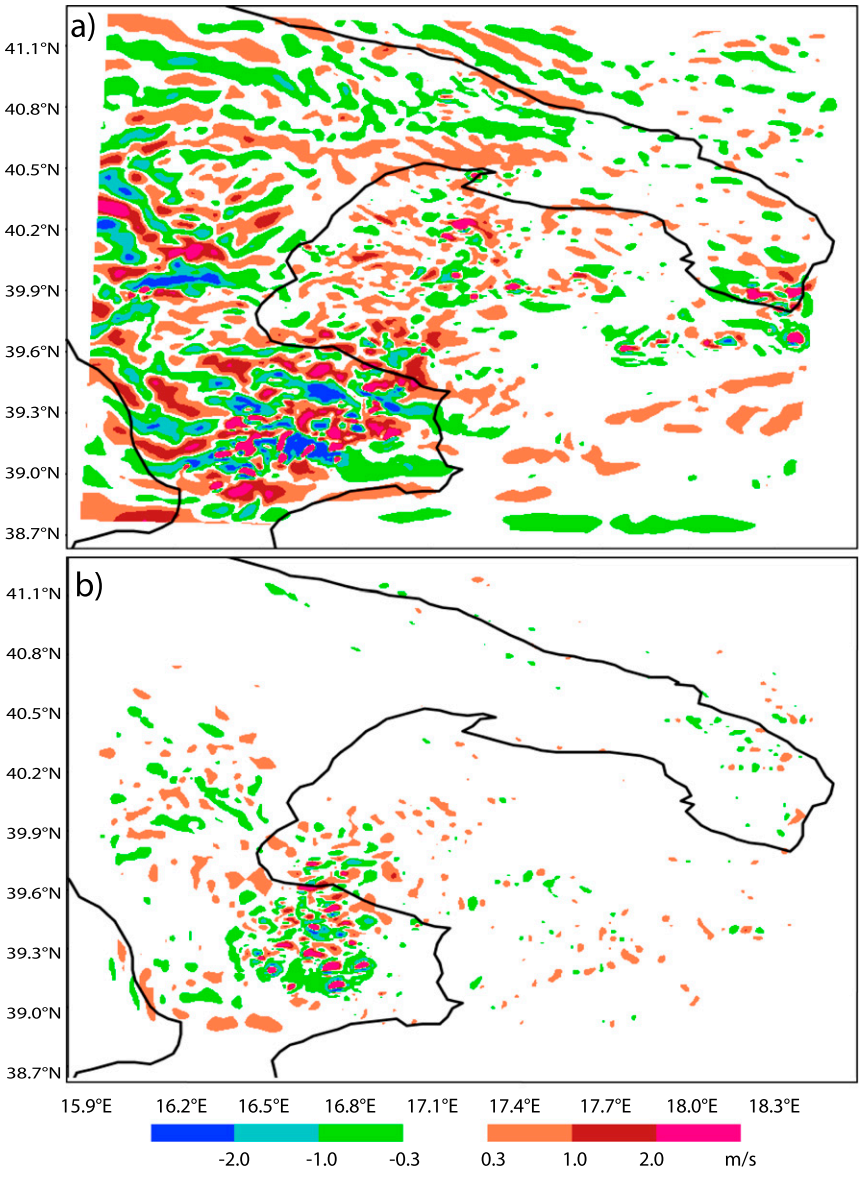

FIG. 10. WRF Model simulation, domain 3. Shown are the vertical velocities (m s^{-1}; color scale) at 700 hPa at 1000 UTC 28 Nov 2012 in the (a) control run and (b) experiment with orography reduced by 80%.

black line in Fig. 2a. It is remarkable that the model is able to reproduce correctly the track and the timing of the supercell over land as well as its weakening near the Murge hills (where again the simulation shows the splitting of the cell) and the new intensification downstream at around 1100 UTC (Fig. 2b), when some EF2 damage was reported near the Adriatic coast (Venerito et al. 2013).

Considering that the predictability of convection is generally limited to a few hours, we expect that the longer forecasting range in this simulation is associated with the presence of a forcing that the model is able to properly represent. This is discussed in the following subsection.

b. *Supercell development*

To better identify the mechanisms responsible for the generation of the supercell, we start by focusing on the time step when the cell appears first (0905 UTC). At that time, the pattern of 800-hPa vertical vorticity in Fig. 9, together with the conditions of convective instability in which the cells develop (Fig. 6) and the in-phase vertical velocity and temperature perturbations (not shown) are hallmarks of horizontal rolls oriented

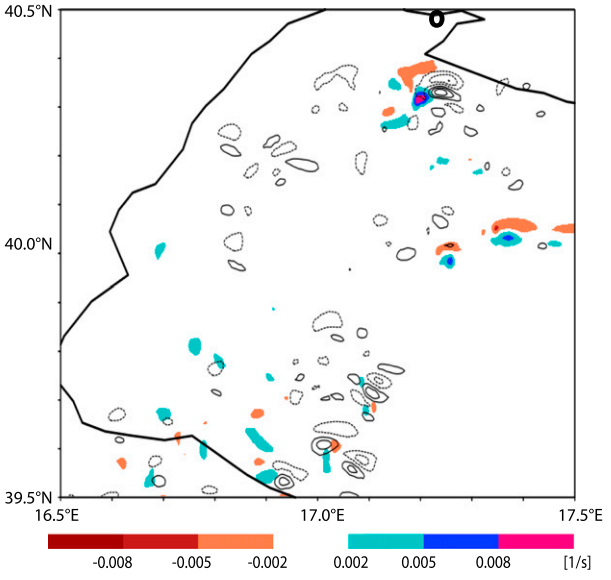

FIG. 11. WRF Model simulation, domain 3. Shown are the vertical vorticities at 800 hPa (s^{-1}; color scale) and at 500 hPa (dashed contours for −0.008, −0.005, and −0.002 s^{-1}; solid contours for 0.002, 0.005, and 0.008 s^{-1}) at 1010 UTC 28 Nov 2012, at the time when the cell reaches its maximum intensity. The location of the tornado landfall is indicated by O.

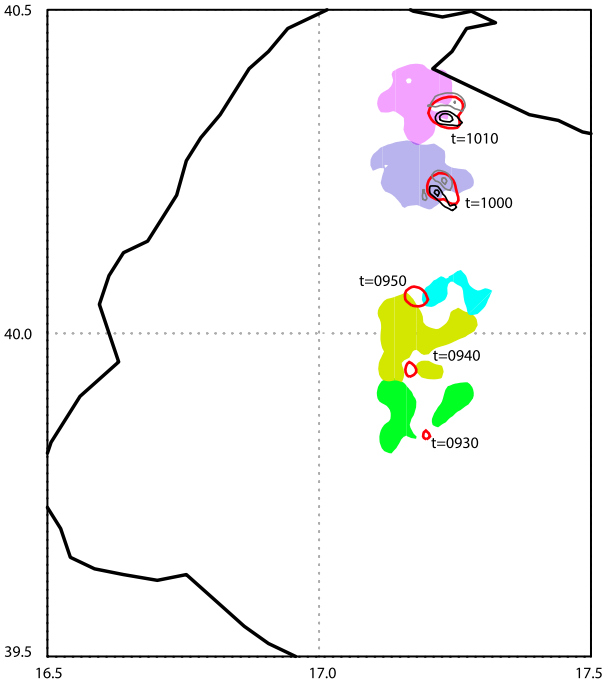

FIG. 12. The evolution of the supercell from 0930 to 1010 UTC as illustrated by the contour of w at 500 hPa = 6 m s^{-1} (red) and the vertical vorticity contours (4 and 8 × 10^{-3} s^{-1}, black; −4 and −8 × 10^{-3} s^{-1}, gray) at 500 hPa. The colored areas indicate a water vapor mixing ratio greater than 7 g kg^{-1} at 800 hPa in an approximately 20 km × 20 km square surrounding the growing cells at the indicated times.

along the boundary layer shear direction, that is, west-southwest–east-northeast (Fig. 5 in Brown 1980). The cloud water content in Fig. 9 shows that the vorticity signatures are not associated with deep convection, but with regions of mesoscale ascent confined in the low levels before storm development. At the eastern terminus (black arrow) of the southern line, which extends from the Sila mountains of Calabria to the southern tip of Apulia across the Ionian Sea, the cell that will develop into the supercell forms.

It is well known that convective rolls may play a key role in the transport of energy and moisture upward; in particular, the associated mesoscale ascent may carry warm and moist air from the surface to the top of the boundary layer, so that they may locally promote the triggering of deep convection in the presence of favorable conditions (Weckwerth et al. 1996, 2004). This is what happens in the lee of the Sila mountains, where the low-level circulations induced by the western end of one of these rolls is superimposed with the intense upper-level perturbations induced by the flow past the orography of Calabria (see the 700-hPa vertical velocity at 1000 UTC in Fig. 10a).

At 1010 UTC, just before landfall, Fig. 11 shows that the supercell reaches intense vertical vorticity both at 800 hPa (colors) and 500 hPa (contours), while the other rolls and/or smaller cells, moving along the Ionian Sea (Fig. 8), do not intensify and their vorticity remains confined in the low levels. The upper-level vertical-vorticity couplets (+/−) in the lee of the orography (Fig. 11) are evidence of updrafts in vertical wind shear (essential for supercell dynamics) for the cells triggered by the orography. However, the simulations indicate that only the cell maintained by the roll-associated moisture perturbation can last long enough to develop into a supercell. Figure 12 follows the cell (updraft) that continues to intensify from 0930 to 1010 UTC and becomes the simulated supercell that makes landfall near Taranto.

As discussed above and emphasized again hereafter, the supercell develops because the environment is extremely favorable for supercell development (and for tornadogenesis). The region where the supercell forms is characterized by a maximum in the 0–1-km shear (Fig. 7) and 0–3-km shear (Fig. 13a, at 0900 UTC), as it is near the left side of the low-level jet, at the border with the wake induced by the orography of Calabria. Next, as the cell moves over the sea, it remains in an environment favorable for rotation: comparing Fig. 13a with Fig. 13b at 1 h apart (in the latter panel, the cell can be identified with the small maximum approaching the coast of Apulia), we can see that the cell (whose track is shown in

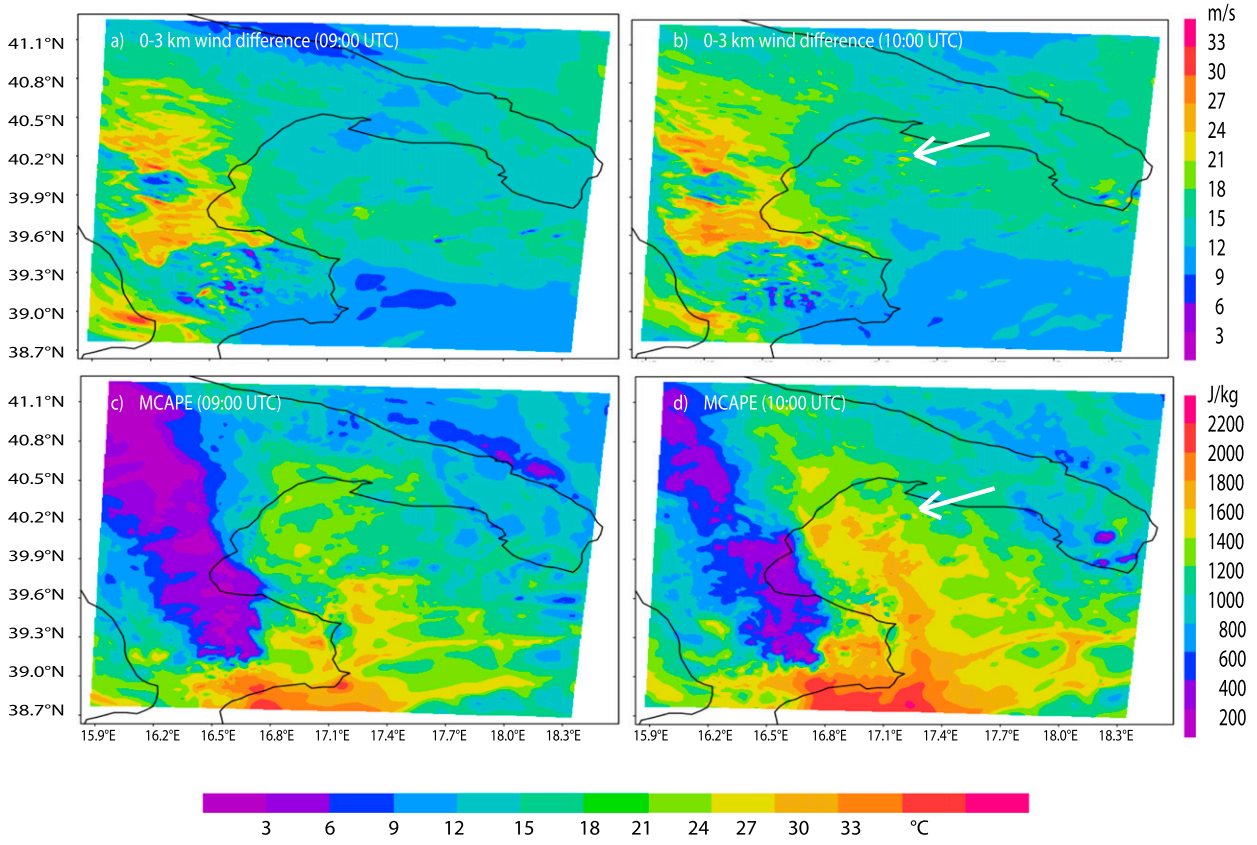

FIG. 13. WRF Model simulation, domain 3. Shown are the 0–3-km wind differences at (a) 0900 and (b) 1000 UTC and maximum CAPE at (c) 0900 and (d) 1000 UTC. The location of the supercell at 1000 UTC is indicated by the arrow.

Fig. 2a) remains inside a band of high 0–3-km shear, as both move northward nearly synchronously.

During its transit across the Ionian Sea, the cell progressively intensifies (Fig. 12). Following the northward extension of the warm tongue, a significant 1-h increase in CAPE up to 1600–1800 J kg^{-1} is simulated in the Ionian Sea (cf. Fig. 13c and Fig. 13d). (Note that the simulated CAPE in Brindisi is about 1000 J kg^{-1} and is consistent with the observed vertical profile, suggesting that the Brindisi sounding does not properly represent the environmental conditions associated with the development of the supercell, because of the strong inhomogeneity in the area.) The supercell develops near the border of the warm tongue; in Fig. 14, the supercell can be identified with the contour line of 600-hPa vertical velocity near 39.8°N, 17.2°E, just north of the region affected by the highest values.

c. *Role of the orography*

The previous analysis suggests that the supercell developed in a complex environment, characterized by rough orography and coastlines. Hereafter, in order to test the hypothesis that the orography played a key role in the generation of the supercell, additional experiments were performed with the orography reduced by 80% and 50%. The reduction to 50% has the effect of weakening the convection induced by the mountain, so that the supercell is weaker (maximum updraft helicity of 80 m^2 s^{-2} compared with 250 m^2 s^{-2} in the control run) but it is still present in the simulation. A reduction to 20% of the original elevation is required to strongly suppress the orographic convection and the generation of the supercell. Figure 15, which is the equivalent of Fig. 7 in the new experiment, does not show leeside vortices, since the incoming flow is no longer blocked by the Sila mountains (in the new experiment $h \approx 400$ m, while U and N are about the same as before and therefore Fr > 1). Thus, a regime of ''flow over'' the orography is favored; on the other hand, the uplift induced by the orography is sufficient to trigger only weak cells (h/LFC $\lessapprox 1$), which do not show any significant low-level rotation.

Figure 10 shows the vertical velocity at 700 hPa in the sensitivity experiment (Fig. 10b) in comparison with the control run (Fig. 10a). It is apparent that in the latter experiment the mountains also perturb the flow far

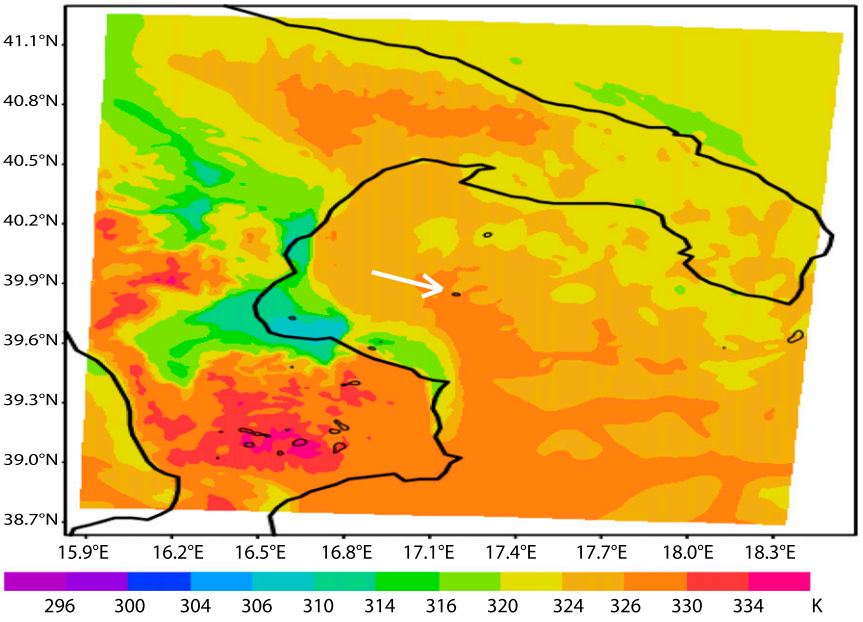

FIG. 14. WRF Model simulation, domain 3. Shown are θ_e results at 1000 hPa (K; color scale) and 600-hPa vertical velocity (contour line = 5 m s^{-1}) at 0930 UTC.

downstream in the Adriatic Sea, where a train of gravity waves is apparent (the presence of mountain waves was particularly clear in the early morning of 28 November), but also on its eastern side over the Ionian Sea, where alternating positive and negative vertical velocity perturbations (red and green stripes perpendicular to the main flow) can be identified in Fig. 10a. In contrast, the case with reduced orography generates very weak perturbations in the vertical velocity (Fig. 10b), producing some weak updrafts only over the Sila mountains and immediately downstream, while weak cells appear over the Ionian Sea. The reduction of the mountain height affects the 0–3-km shear, which is strongly reduced in the sensitivity experiment, mainly because of the weaker upper-level winds (not shown). This means that the shear responsible for the generation of the horizontal rolls is no longer present and only weak convective cells are generated over the sea. At the same time, the reduced environmental shear is detrimental to the generation of rotation in the cells.

6. Conclusions

Numerical simulations are performed with the WRF Model for one of the most intense tornado situations in Europe in the last few years: an EF3 tornado affecting the surroundings of the city of Taranto in southeastern Italy on 28 November 2012. Considering that the grid spacing of the inner grid is 1 km, our focus is on the supercell spawning the tornado in Taranto and not on the tornado itself. The numerical experiment shows that it is possible to reproduce the track and the change in intensity, as well as the timing of the supercell.

The genesis of the supercell is due to a combination of mesoscale flow features and topographic flow effects, which are illustrated in Fig. 16:

- the mesoscale flow features, high-θ_e low-level air and cold midtropospheric air, produce potential instability in the Ionian Sea;
- the orography of Calabria (Sila mountains) plays a key role in triggering convection over the mountains and downstream;
- the strong deep-layer and low-level wind shear produce an environment favorable, respectively, for supercell and tornado development, with high values concentrated in a band that surrounds the supercell during its evolution. Also, the low-level (boundary layer) shear is responsible for the generation of convective rolls, which move northward along the Ionian Sea, locally creating conditions even more favorable for the triggering and maintenance of convection.

The supercell is triggered where the upper-level perturbations generated by the mountains are superimposed with the western end of one of these rolls, which delimits a tongue of very moist and warm air at its northern border. We are not aware that similar mechanisms for supercell triggering have been previously identified elsewhere.

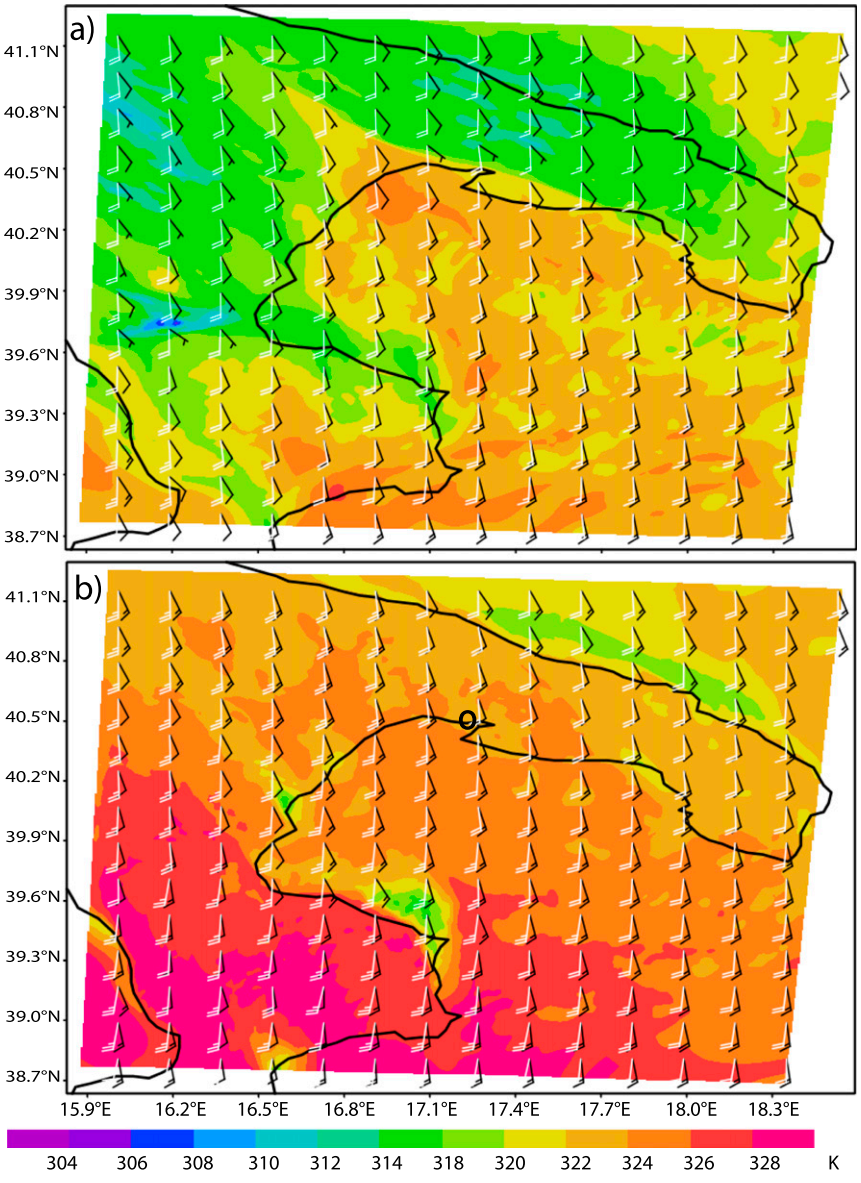

FIG. 15. As in Fig. 7, but for the experiment with the orography reduced by 80%.

Considering that the predictability of convection is generally limited to a few hours, we believe that the skill of the simulation in representing the supercell development is associated with the key role of the orographic forcing, which the model is able to properly represent. This role was better identified by comparing the control run with a sensitivity experiment implemented by reducing the mountain height by 80%. The lower orography has the effect of reducing the orographic uplift and the consequent triggering of convection, as well as the low-level vorticity in the Ionian Sea and, thus, the convective rolls.

Together with the favorable environmental conditions and the orography, other forcings may have affected the development of the supercell. In particular, we believe that the thermodynamic changes induced by the positive sea surface temperature anomaly (Vautard et al. 2016) during the event (around 2°C) enhanced the lower-tropospheric instability and made deep convection possible even during an unusual period of the year for such events, like the end of November (see, e.g., Meredith et al. 2015). Additional experiments with modified sea temperature (in progress) will shed further light on this sensitivity, which may also be relevant to analyze from a climate change perspective.

The interest in this specific case study is not limited to the peculiar environmental conditions where the tornado

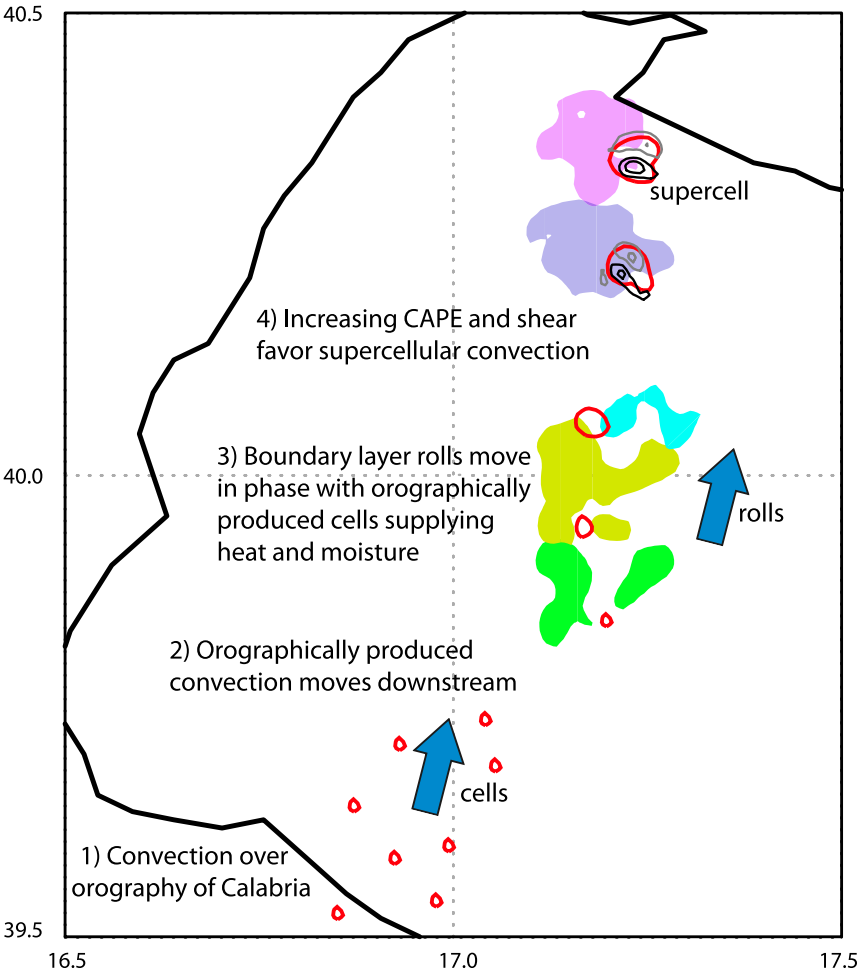

FIG. 16. Schematic diagram of the principal factors contributing to the simulated Taranto supercell: 1) orographic convection over Calabria triggers intense updraft cells, which 2) move downstream in the direction of Taranto, while 3) a heat-and-moisture-supplying boundary layer roll, moving in the same direction at about the same speed, comes into phase with one of the cells that 4) grows into a supercell as CAPE and vertical wind shear become more favorable. See Fig. 12 for definitions of the contours and color shading.

developed, but is also related to the recursive occurrence of similar events in southern Apulia. Gianfreda et al. (2005) have documented tornadoes in this region since the sixteenth century, some of which were very intense. More recently, other events have been identified near the port of Taranto (26 October 2010 and 27 January 2011) or along the Ionian coast of Apulia (the EF2 tornado outbreak documented in Monacizzo, Ginosa, and Carosino on 12 November 2014 and the tornado in Gallipoli on 19 November 2013). The analysis of the Italian radar reflectivity mosaic map for the latter two cases, which will be the subject of a forthcoming study, reveals the possible presence of a mechanism of development similar to the one studied here, as it shows a line of convective cells elongated from the Sila mountains in the SW–NE direction. Thus, the identification of this pattern can be considered as a diagnostic signal relevant to the possible occurrence and location of such severe events for nowcasting purposes.

Finally, we hope that the present study may promote the analysis of other severe tornadoes in the Mediterranean basin. Numerical simulations will need to be performed in several cases to analyze the relevant forcings responsible for the generation and intensification of the supercells, to identify the patterns conducive to risk, and to determine the existence of possible analogies among mechanisms active in different regions.

Acknowledgments. The stay of MMM in Boulder was supported by NCAR. The present work developed within the framework of the Comparison of Tornadic Supercells and Their Environmental Conditions in

Japan and Italy project, a joint initiative between the Japan Society for the Promotion of Science (JSPS) and the National Research Council (CNR) for the period 2016–17. Figure 8 was produced with VAPOR (www.vapor.ucar.edu). MMM gratefully acknowledges William Gallus for stimulating discussions.

REFERENCES

Antonescu, B., D. Schultz, F. Lomas, and T. Kühne, 2016: Tornadoes in Europe: Synthesis of the observational datasets. *Mon. Wea. Rev.*, **144**, 2445–2480, doi:10.1175/MWR-D-15-0298.1.

Aran, M., J. Amaro, J. Arús, J. Bech, F. Figuerola, M. Gayà, and E. Vilaclara, 2009: Synoptic and mesoscale diagnosis of a tornado event in Castellcir, Catalonia, on 18th October 2006. *Atmos. Res.*, **93**, 147–160, doi:10.1016/j.atmosres.2008.09.031.

ARPAV, 2015: Temporali intensi di mercoledì 8 luglio 2015 sul Veneto. Agenzia Regionale per la Prevenzione e Protezione Ambientale del Veneto Rep., 11 pp. [Available online at http://www.arpa.veneto.it/temi-ambientali/meteo/riferimenti/documenti/documenti-meteo/Relazionetornadosulveneto08_07_15.pdf/view.]

Bech, J., R. Pascual, T. Rigo, N. Pineda, J. M. López, J. Arús, and M. Gayà, 2007: An observational study of the 7 September 2005 Barcelona tornado outbreak. *Nat. Hazards Earth Syst. Sci.*, **7**, 129–139, doi:10.5194/nhess-7-129-2007.

Bertato, M., D. B. Giaiotti, A. Manzato, and F. Stel, 2003: An interesting case of tornado in Friuli-northeastern Italy. *Atmos. Res.*, **67–68**, 3–21, doi:10.1016/S0169-8095(03)00043-7.

Bosart, L. F., A. Seimon, K. D. LaPenta, and M. J. Dickinson, 2006: Supercell tornadogenesis over complex terrain: The Great Barrington, Massachusetts, tornado on 29 May 1995. *Wea. Forecasting*, **21**, 897–922, doi:10.1175/WAF957.1.

Brooks, H. E., J. W. Lee, and J. P. Craven, 2003: The spatial distribution of severe thunderstorm and tornado environments from global reanalysis data. *Atmos. Res.*, **67–68**, 73–94, doi:10.1016/S0169-8095(03)00045-0.

Brown, R. A., 1980: Longitudinal instabilities and secondary flows in the planetary boundary layer–A review. *Rev. Geophys. Space Phys.*, **18**, 683–697, doi:10.1029/RG018i003p00683.

Ching, J., R. Rotunno, M. A. LeMone, A. Martilli, B. Kosovic, P. A. Jimenez, and J. Dudhia, 2014: Convectively induced secondary circulations in fine-grid mesoscale numerical weather prediction models. *Mon. Wea. Rev.*, **142**, 3284–3302, doi:10.1175/MWR-D-13-00318.1.

Doswell, C. A., III, G. W. Carbin, and H. E. Brooks, 2012: The tornadoes of spring 2011 in the USA: An historical perspective. *Weather*, **67**, 88–94, doi:10.1002/wea.1902.

Dudhia, J., 1989: Numerical study of convection observed during the Winter Monsoon Experiment using a mesoscale two-dimensional model. *J. Atmos. Sci.*, **46**, 3077–3107, doi:10.1175/1520-0469(1989)046<3077:NSOCOD>2.0.CO;2.

Giaiotti, D. B., M. Giovannoni, A. Pucillo, and F. Stel, 2007: The climatology of tornadoes and waterspouts in Italy. *Atmos. Res.*, **83**, 534–541, doi:10.1016/j.atmosres.2005.10.020.

Gianfreda, F., M. M. Miglietta, and P. Sansò, 2005: Tornadoes in southern Apulia (Italy). *Nat. Hazards*, **34**, 71–89, doi:10.1007/s11069-004-1966-3.

Grams, J. S., R. L. Thompson, D. V. Snively, J. A. Prentice, G. M. Hodges, and L. J. Reames, 2012: A climatology and comparison of parameters for significant tornado events in the United States. *Wea. Forecasting*, **27**, 106–123, doi:10.1175/WAF-D-11-00008.1.

Homar, V., M. Gayà, R. Romero, C. Ramis, and S. Alonso, 2003: Tornadoes over complex terrain: An analysis of the 28th August 1999 tornadic event in eastern Spain. *Atmos. Res.*, **67–68**, 301–317, doi:10.1016/S0169-8095(03)00064-4.

Janjić, Z. I., 2001: Nonsingular implementation of the Mellor–Yamada level 2.5 scheme in the NCEP Meso model. NCEP Tech. Rep. 437, 61 pp. [Available online at http://www2.mmm.ucar.edu/wrf/users/phys_refs/SURFACE_LAYER/eta_part4.pdf.]

Lilly, D. K., 1990: Numerical prediction of thunderstorm—Has its time come? *Quart. J. Roy. Meteor. Soc.*, **116**, 779–798, doi:10.1002/qj.49711649402.

Lionello, P., and Coauthors, 2006: The Mediterranean climate: An overview of the main characteristics and issues. *Mediterranean Climate Variability*, P. Lionello, P. Malanotte-Rizzoli, and R. Boscolo, Eds., Elsevier, 1–26.

Markowski, P. M., and Y. Richardson, 2010: *Mesoscale Meteorology in Midlatitudes.* Wiley-Blackwell, 424 pp.

——, and N. Dotzek, 2011: A numerical study of the effects of orography on supercells. *Atmos. Res.*, **100**, 457–478, doi:10.1016/j.atmosres.2010.12.027.

Mateo, J., D. Ballart, C. Brucet, M. Aran, and J. Bech, 2009: A study of a heavy rainfall event and a tornado outbreak during the passage of a squall line over Catalonia. *Atmos. Res.*, **93**, 131–146, doi:10.1016/j.atmosres.2008.09.030.

Matsangouras, I. T., P. T. Nastos, and I. Pytharoulis, 2012: Numerical investigation of the role of topography in tornado events in Greece. *Advances in Meteorology, Climatology and Atmospheric Physics*, C. G. Helmis and P. T. Nastos, Eds., Springer, 209–215, doi:10.1007/978-3-642-29172-2_30.

——, I. Pytharoulis, and P. T. Nastos, 2014: Numerical modeling and analysis of the effect of complex Greek topography on tornadogenesis. *Nat. Hazards Earth Syst. Sci.*, **14**, 1905–1919, doi:10.5194/nhess-14-1905-2014.

——, P. T. Nastos, and I. Pytharoulis, 2016: Study of the tornado event in Greece on March 25, 2009: Synoptic analysis and numerical modeling using modified topography. *Atmos. Res.*, **169**, 566–583, doi:10.1016/j.atmosres.2015.08.010.

McDonald, J., and K. C. Mehta, 2006: A recommendation for an enhanced Fujita scale (EF-scale), revision 2. Wind Science and Engineering Research Center Rep., Texas Tech University, 111 pp. [Available online at http://www.spc.ncep.noaa.gov/efscale/ef-ttu.pdf.]

Meredith, E. P., V. A. Semenov, D. Maraun, W. Park, and A. V. Chernokulsky, 2015: Crucial role of Black Sea warming in amplifying 2012 Krymsk precipitation extreme. *Nat. Geosci.*, **8**, 615–620, doi:10.1038/ngeo2483.

Miglietta, M. M., and R. Rotunno, 2009: Numerical simulations of conditionally unstable flows over a ridge. *J. Atmos. Sci.*, **66**, 1865–1885, doi:10.1175/2009JAS2902.1.

——, and ——, 2016: An EF3 multivortex tornado over the Ionian region: Is it time for a dedicated warning system over Italy? *Bull. Amer. Meteor. Soc.*, **97**, 337–344, doi:10.1175/BAMS-D-14-00227.1.

——, A. Manzato, and R. Rotunno, 2016: Characteristics and predictability of a supercell during HyMeX SOP1. *Quart. J. Roy. Meteor. Soc.*, **142**, 2839–2853, doi:10.1002/qj.2872

Mlawer, E. J., S. J. Taubman, P. D. Brown, M. J. Iacono, and S. A. Clough, 1997: Radiative transfer for inhomogeneous atmosphere: RRTM, a validated correlated-k model for the longwave. *J. Geophys. Res.*, **102**, 16 663–16 682, doi:10.1029/97JD00237.

Moscatello, A., M. M. Miglietta, and R. Rotunno, 2008: Numerical analysis of a Mediterranean ''hurricane'' over southeastern Italy. *Mon. Wea. Rev.*, **136**, 4373–4397, doi:10.1175/2008MWR2512.1.

Nastos, P. T., and I. T. Matsangouras, 2014: Analysis of synoptic conditions for tornadic days over western Greece. *Nat. Hazards Earth Syst. Sci.*, **14**, 2409–2421, doi:10.5194/nhess-14-2409-2014.

Niu, G.-Y., and Coauthors, 2011: The community Noah land surface model with multiparameterization options (Noah-MP): 1. Model description and evaluation with local-scale measurements. *J. Geophys. Res.*, **116**, D12109, doi:10.1029/2010JD015139.

Peterson, R. E., 1998: A historical review of tornadoes in Italy. *J. Wind Eng. Ind. Aerodyn.*, **74–76**, 123–130, doi:10.1016/S0167-6105(98)00010-5.

Schwartz, C. S., G. S. Romine, R. A. Sobash, K. R. Fossell, and M. L. Weisman, 2015: NCAR's experimental real-time convection-allowing Ensemble Prediction System. *Wea. Forecasting*, **30**, 1645–1654, doi:10.1175/WAF-D-15-0103.1.

Skamarock, W. C., and Coauthors, 2008: A description of the Advanced Research WRF version 3. NCAR Tech. Note NCAR/TN-475+STR, 113 pp., doi:10.5065/D68S4MVH.

Smith, R. B., 1979: The influence of mountains on the atmosphere. *Advances in Geophysics*, Vol. 21, Academic Press, 87–230.

Smolarkiewicz, P. K., and R. Rotunno, 1989: Low Froude number flow past three-dimensional obstacles. Part I: Baroclinically generated lee vortices. *J. Atmos. Sci.*, **46**, 1154–1164, doi:10.1175/1520-0469(1989)046<1154:LFNFPT>2.0.CO;2.

Thompson, G., P. R. Field, R. M. Rasmussen, and W. D. Hall, 2008: Explicit forecasts of winter precipitation using an improved bulk microphysics scheme. Part II: Implementation of a new snow parameterization. *Mon. Wea. Rev.*, **136**, 5095–5115, doi:10.1175/2008MWR2387.1.

Vautard, R., P. Yiou, F. E. L. Otto, P. A. Stott, N. Christidis, G. J. Van Oldenborgh, and N. Schaller, 2016: Attribution of human-induced dynamical and thermodynamical contributions in extreme weather events. *Environ. Res. Lett.*, **11**, 114009, doi:10.1088/1748-9326/11/11/114009.

Venerito, M., P. Fago, C. Colella, R. Laviano, F. Montanaro, P. Sansò, and G. Mastronuzzi, 2013: Il tornado di Taranto del 28 novembre 2012: percorso, orografia e vulnerabilità. *Geologia dell'Ambiente*, No. 4/2013, Società Italiana di Geologia Ambientale, Rome, Italy, 2–9. [Available online at http://www.sigeaweb.it/documenti/gda/gda-4-2013.pdf.]

Weckwerth, T. M., J. W. Wilson, and R. M. Wakimoto, 1996: Thermodynamic variability within the convective boundary layer due to horizontal convective rolls. *Mon. Wea. Rev.*, **124**, 769–784, doi:10.1175/1520-0493(1996)124<0769:TVWTCB>2.0.CO;2.

——, and Coauthors, 2004: An overview of the International H_2O Project (IHOP_2002) and some preliminary highlights. *Bull. Amer. Meteor. Soc.*, **85**, 253–277, doi:10.1175/BAMS-85-2-253.

Weisman, M. L., and J. B. Klemp, 1982: The dependence of numerically simulated convective storms on wind shear and buoyancy. *Mon. Wea. Rev.*, **110**, 504–520, doi:10.1175/1520-0493(1982)110<0504:TDONSC>2.0.CO;2.

Wyngaard, J. C., 2004: Toward numerical modeling in the ''terra incognita.'' *J. Atmos. Sci.*, **61**, 1816–1826, doi:10.1175/1520-0469(2004)061<1816:TNMITT>2.0.CO;2.